Integrating factor techniques applied to the Schrödinger-like equations. Comparison with Split-Step methods

Martino Lovisetto [*], Didier Clamond, Bruno Marcos

Université Côte d'Azur, CNRS UMR 7351, LJAD, Parc Valrose, 06108 Nice cedex 2, France

ARTICLE INFO

ABSTRACT

The nonlinear Schrödinger and the Schrödinger–Newton equations model many phenomena in various fields. Here, we perform an extensive numerical comparison between splitting methods (often employed to numerically solve these equations) and the integrating factor technique, also called Lawson method. Indeed, the latter is known to perform very well for the nonlinear Schrödinger equation, but has not been thoroughly investigated for the Schrödinger–Newton equation. Comparisons are made in one and two spatial dimensions, exploring different boundary conditions and parameters values. We show that for the short range potential of the nonlinear Schrödinger equation, the integrating factor technique performs better than splitting algorithms, while, for the long range potential of the Schrödinger–Newton equation, it depends on the particular system considered.

1. Introduction

The nonlinear Schrödinger and the Schrödinger–Newton (also called Schrödinger–Poisson) equations describe a large number of phenomena in different physical domains. These equations are nonlinear variants of the Schrödinger one, which, in non-dimensional units, reads

$$i\,\partial_t\,\psi \,+\, \tfrac{1}{2}\,\nabla^2\psi \,-\, V\,\psi \,=\, 0, \tag{1}$$

where ψ is a function of space and time, ∇^2 is the Laplace operator and V is a function of ψ, space and time.

For the nonlinear Schrödinger equation (hereafter NLS), the *local nonlinear* potential is

$$V \,=\, g\,|\psi|^2, \tag{2}$$

where g is a coupling constant. For $g > 0$ the interaction is repulsive, while it is attractive for $g < 0$. The NLS equation describes various physical phenomena, such as Bose–Einstein condensates [1], laser beams in some nonlinear optical media [2], water wave packets [3], etc.

In the case of the Schrödinger–Newton (SN) equation, the potential is given by the Poisson equation

$$\nabla^2 V \,=\, g\,|\psi|^2, \tag{3}$$

* Corresponding author.
E-mail address: Martino.LOVISETTO@univ-cotedazur.fr (M. Lovisetto).

where g is a coupling constant, the interaction being attractive if $g > 0$ and repulsive if $g < 0$. It is therefore *nonlinear* and *nonlocal*, giving rise to collective phenomena [4], appearing for instance in optics [5–7], Bose–Einstein condensates [8], astrophysics and cosmology [9–11] and theories describing the quantum collapse of the wave function [12,13]. It is also employed as a model for conducting semi-classical cosmological simulations [14].

The SN equation takes a slightly different form when applied in cosmology [15]. Here, due to the expansion of the universe, the Poisson equation is modified [16] as

$$\nabla^2 V = a^{-1} g \left(|\psi|^2 - 1 \right), \tag{4}$$

where $a(t)$ is a scaling factor. The modification of the Poisson equation (4) ensures that the potential is finite in an infinite universe [15]. From a numerical perspective, when solving the Poisson equation in Fourier space, this term effectively eliminates the singularity associated with the $k = 0$ mode.

These NLS and SN equations are special cases of the Gross–Pitaevskii–Poisson (GPP) equation

$$i \partial_t \psi + \tfrac{1}{2} \nabla^2 \psi - V_1 \psi - V_2 \psi = 0, \qquad \nabla^2 V_1 = g_1 |\psi|^2, \qquad V_2 = g_2 |\psi|^2. \tag{5}$$

This equation appears in many fields, such as optics [17,18], Bose-Einstein condensates [19] and cosmology (to simulate scalar field dark matter) [20–22].

In order to solve the above equations, except for very special cases, numerical methods must be used. Two families of temporal numerical schemes are commonly used to solve the Schrödinger equation with a nonlinear potential: the integrating factor technique (generally attached with a Runge–Kutta scheme) and the Split-Step method. In this paper, we present an extensive comparison between integrating factor methods and splitting algorithms, considering both accuracy and computational speed. Comparisons are made exploring different types of boundary conditions, in one and two spatial dimensions, with parameters ranging in values close to many regimes of physical interest. The main reason for choosing these methods is that, in the literature, Split-Step solvers are commonly used to integrate both the SN and the NLS equations [23,24], while the integrating factor has been applied to integrate the NLS with very performing results [25,26]. A natural question, which is also the main motivation of this work, is how the integrating factor technique performs when considering the long range interactions of the SN system instead of short range ones of the NLS. We show that the integrating factor performs better than splitting algorithms for local interactions (such as the NLS). When a long range interaction (such as the one appearing in the SN equation) is considered, the relative performance between the integrating factor and splitting algorithms depends on the system.

The paper is organized as follows. In section 2, the methods of numerical time integration are described. Section 3 concerns detailed comparisons between Split-Step integrators (order 2, 4 and 6 with fixed time-step and order 4 with adaptive time-step) and standard algorithms with adaptive time-step belonging to the Runge–Kutta family [27–29] together with the integrating factor technique. Conclusions are drawn in section 4.

2. Numerical algorithms

In this section, we describe the different numerical methods used for the temporal resolution of the equations considered in the paper. First, we outline the integrating factor technique attached with an adaptive embedded scheme of arbitrary order. Then, we describe the Split-Step algorithm, with both fixed and adaptive time-step.

Spatial resolution are performed with pseudo-spectral methods. In particular, we rely on methods based on fast Fourier transform (FFT) due to their efficiency and accuracy [30].

2.1. Integrating factor

The integrating factor method can be applied to any differential equation of the form

$$i \partial_t \psi = F(\boldsymbol{r}, t, \psi), \qquad \psi = \psi(\boldsymbol{r}, t), \tag{6}$$

where the right-hand side can be split into linear and nonlinear parts. This results in

$$i \partial_t \psi + \mathcal{L} \psi = \mathcal{N}(\boldsymbol{r}, t, \psi), \tag{7}$$

where $\mathcal{L}$ is an easily computable (generally autonomous) linear operator and $\mathcal{N} \stackrel{\text{def}}{=} F + \mathcal{L}\psi$ is the remaining (usually) nonlinear part. At the n-th time-step, with $t \in [t_n, t_{n+1}]$, the change of dependent variable

$$\phi \stackrel{\text{def}}{=} \exp\left[(t - t_n)\mathcal{L}\right] \psi \qquad \Longrightarrow \qquad i \partial_t \psi = \exp\left[(t_n - t)\mathcal{L}\right] \left(i \partial_t \phi - \mathcal{L}\phi \right), \tag{8}$$

yields the equation

$$i \partial_t \phi = \exp\left[(t - t_n)\mathcal{L}\right] \mathcal{N}. \tag{9}$$

Note that this change of variable is such that $\phi = \psi$ at $t = t_n$. By selecting an appropriate operator $\mathcal{L}$, it is possible to significantly mitigate the stiffness in (7). Consequently, during the time interval $t \in [t_n; t_{n+1}]$, it is possible to obtain a satisfactory approximation

of equation (9) using algebraic polynomials. As a result, conventional time-stepping techniques prove to be effective in efficiently solving (9). Here, we focus on adaptive Runge–Kutta methods [29,31].

As explained in [32], it is possible to further improve and optimize the integrating factor method. The details of this improved version of the integrating factor technique are illustrated in Appendix A. We perform our numerical tests using this optimized version of the integrating factor technique, which hereafter is denoted as IFC.

2.1.1. Application to the Schrödinger equation

Applying these methods to the Schrödinger equation (1) is a simple and direct process. Specifically, for the SN and NLS equations, the Laplacian term is a linear operator while the potential V is a nonlinear operator. When transitioning into Fourier space in the positional domain, the equation transforms into

$$\mathrm{i}\,\partial_t \widehat{\psi} \;-\; \tfrac{1}{2}\,k^2\,\widehat{\psi} \;-\; \widehat{V\psi} \;=\; 0, \tag{10}$$

where symbols represented by 'hats' indicate that the Fourier transforms pertain to the underlying quantity, while 'k' is defined as the magnitude of the vector 'k,' referred to as the wavenumber. Hence, the system has been structured in a way that makes the application of the integrating factor technique straightforward. With the change of variable $\phi(\mathbf{k},t)=\widehat{\psi}(\mathbf{k},t)\,\mathrm{e}^{\mathrm{i}k^2(t-t_0)/2}$, one obtains

$$\partial_t \phi \;=\; -\mathrm{i}\,\mathrm{e}^{\mathrm{i}k^2(t-t_0)/2}\,\widehat{V\psi}\,. \tag{11}$$

In order to perform our numerical tests, we use the Dormand and Prince 5(4) [27] and Tsitouras 5(4) [28] integrators. Both schemes are Runge–Kutta pairs of order 5(4). However, we observe a speed difference between these solvers of maximum 10%, depending on the simulated system. For this reason, we choose for each case the fastest of the two: specifically for NLS and the periodical SN equations we use the Dormand and Prince scheme, while in all the other cases we rely on Tsitouras' one. The higher-order Fehlberg 7(8) integrator [29] is also used as *reference solutions* for accuracy comparisons (see section 3.1).

2.2. Split-Step methods

The Split-Step method [33] performs the temporal resolution of the Schrödinger equation separating the linear terms from the nonlinear ones, in a different manner compared with the integrating factor. Writing the equation as

$$\mathrm{i}\,\partial_t \psi \;=\; H\,\psi, \tag{12}$$

$H=-\tfrac{1}{2}\nabla^2 + V$ being the Hamiltonian operator, the formal solution is

$$\psi(\mathbf{r},t) \;=\; \exp\left(-\mathrm{i}\int_{t_n}^{t} H\,\mathrm{d}t\right)\psi(\mathbf{r},t_n), \qquad t\in[t_n;t_{n+1}]. \tag{13}$$

Except for very few cases, the result of the operator $\exp\left(-\mathrm{i}\int_{t_n}^{t} H\,\mathrm{d}t\right)$ applied to $\psi(\mathbf{r},t_n)$ is unknown. Nevertheless, for $t\in[t_n;t_{n+1}]$, it is possible to approximate $\exp\left(-\mathrm{i}\int_{t_n}^{t} H\,\mathrm{d}t\right)$ as a product of exponentials, each one involving either the potential or the Laplacian term, with appropriate coefficients. For example, the approximation corresponding to the Split-Step method of order 2 is

$$\mathrm{e}^{-\int_{t_n}^{t}\mathrm{i}H\,\mathrm{d}t} \;=\; \mathrm{e}^{-\mathrm{i}K(t-t_n)/2}\,\mathrm{e}^{-\int_{t_n}^{t}\mathrm{i}V\,\mathrm{d}t}\,\mathrm{e}^{-\mathrm{i}K(t-t_n)/2} \;+\; O\left((t-t_n)^2\right), \tag{14}$$

where $K=-\tfrac{1}{2}\nabla^2$.

At higher orders, the approximation of the operator $\exp\left(-\mathrm{i}\int_{t_n}^{t} H\,\mathrm{d}t\right)$ is known as Suzuki-Trotter expansion [34]. It is generally more complicated than (14) and not unique, which can be determined with the Baker–Campbell–Hausdorff formula [24]. For our numerical tests, we consider the Split-Step of orders 2, 4 and 6, whose pseudo-codes are listed in Appendix B.

It is possible to design an adaptive time-step scheme with Split-Step methods. Here, we consider an adaptive embedded splitting pair [35] of order 4(3). This algorithm is characterized by a fourth-order splitting solver derived by Blanes and Moan [36] embedded with third order scheme constructed by Thalhammer and Abhau [35,23]. The pseudo-code for this algorithm, hereafter denoted "SSa", is described in Appendix B.

3. Numerical comparison of the different time-integrators

In this section, we compare the efficiencies of the methods previously described. The comparisons focus on speed and accuracy of each algorithm, simulating systems with different potentials, boundary conditions and physical regimes. Speed is measured with the total time needed to run each simulation, which represents the time duration measured from the initiation of the simulation at $t=0$ until it reaches the specified final time, t_{fin}. To ensure accuracy and reliability, all experiments were conducted on the same computing cluster. We mitigated potential fluctuations in CPU performance by averaging the time measurements over 10 independent runs of each simulation. First, we outline the different estimators employed to determine the accuracy of each numerical integrator. Then, we list and summarize the results for every equations considered, in one and two spatial dimensions. We start with the

NLS equation which is used as benchmark, since an analytical solution is known in the one dimensional case. Then we switch to the SN equation with both open and periodic boundary conditions. Finally, we present the results for the two dimensional Gross–Pitaevskii–Poisson equation, which can be considered as a hybrid version of the SN and NLS systems.

3.1. Estimators of the accuracy of the time-integration algorithms

The accuracy of each time-integration algorithm is estimated looking at three different indicators:

1. The energy conservation. The energy E is a constant of motion for the Schrödinger equation. For the NLS and SN equations, it is defined as

$$E = \frac{1}{2} \int d\boldsymbol{r}\, \psi^* \left(-\nabla^2 + V\right) \psi. \tag{15}$$

Using the initial energy as reference, the error on the energy conservation is

$$\Delta E_i = \left| \frac{E(t_i)}{E(t_0)} - 1 \right|, \tag{16}$$

where t_0 is the initial time and t_i denotes the i-th time-step of the numerical integration. This error being (in general) time-dependent, we consider the error

$$\overline{\Delta E} = \max_i \left[\Delta E_i \right], \tag{17}$$

the latter being the maximal difference with respect to the initial value, during the whole simulation.
2. Another constant of motion for the considered equation, is the mass,

$$M = \int d\boldsymbol{r}\, |\psi|^2. \tag{18}$$

This quantity is automatically conserved with machine precision when using splitting algorithms, while it is not in general the case with the integrating factor. For this reason, when the latter technique is employed, we impose mass conservation at each time-step, multiplying the solution ψ by $M_0 / \int d\boldsymbol{r}\, |\psi|^2$, where M_0 is the initial mass.
3. The error on the solution performing time reversion tests. This quantity is obtained running a simulation up to a given time t_{fin}, then reversing the time and evolving back to the initial instant. The error is monitored using the L_∞-norm of the difference between the solution at the initial time, at beginning of the simulation and at the end of it. Denoting the "backward" solution by ψ_{backward}, one has

$$\Delta \psi_{\text{rev}} = \max_i \left(\left| \psi(x_i, t_0) - \psi_{\text{backward}}(x_i, t_0) \right| \right). \tag{19}$$

4. The two estimators above favorize *a priori* time-splitting algorithms because they are symplectic and reversible, whereas the integrating factor is not. For this reason, we also compare the result of the simulations with a "reference one", very accurate, using an adaptive Fehlberg integrator of order 7 embedded within an order 8 scheme, with a very small tolerance, $\text{tol} = 10^{-14}$. Defining this estimator as $\Delta \psi_{\text{ref}}$, one has

$$\Delta \psi_{\text{ref}} = \max_i \left(\left| \psi(x_i, t_f) - \psi_{\text{F7(8)}}(x_i, t_{\text{fin}}) \right| \right), \tag{20}$$

where ψ is the numerical solution provided by the particular method considered and $\psi_{\text{F7(8)}}$ is the one outputted by the Fehlberg 7(8) integrator.

3.2. 1D nonlinear Schrödinger equation

We first consider the case of the one dimensional NLS

$$i \frac{\partial \psi}{\partial t} + \frac{1}{2} \frac{\partial^2 \psi}{\partial x^2} + |\psi|^2 \psi = 0, \tag{21}$$

which admits a simple analytical solution

$$\psi(x, t) = \sqrt{2}\, \text{sech}\left(\sqrt{2}\, x\right) \exp(i\, t). \tag{22}$$

We present a set of simulations in order to compare the Split-Step integrators with the IFC, looking at the energy conservation error, the error on the solution and the total time needed to run each simulation. In these simulations, the space is discretized with $N = 2048$ points, in a domain of length $L = 80$ and the analytical solution at $t = 0$ is used as initial condition. The results are summarized in Table 1. We observe that the IFC solver is the fastest one by at least a factor 2, presenting at the same time the best results to all the indicators: it uses a larger time-step, presents equal or better energy conservation, returns only a slightly worse $\Delta \psi_{\text{rev}}$ and it is one of the best comparing to the reference simulation.

Table 1

Comparison for the 1D NLS equation between the IFC method and the Split-Step solvers. T is the total time required to run each simulation, measured in seconds. The Δt for adaptive algorithms is the averaged one.

Method	Δt	$\overline{\Delta E}$	$\Delta \psi_{\text{rev}}$	$\Delta \psi_{\text{ref}}$	$T(s)$
SS2	10^{-3}	$7.5 \cdot 10^{-13}$	$6.3 \cdot 10^{-10}$	$1.1 \cdot 10^{-4}$	86.7
SS4	$5 \cdot 10^{-3}$	10^{-15}	$8.2 \cdot 10^{-10}$	$5.8 \cdot 10^{-7}$	38.1
SS6	$2 \cdot 10^{-2}$	10^{-15}	$2.0 \cdot 10^{-10}$	$3.7 \cdot 10^{-9}$	29.3
SSa, tol $= 10^{-6}$	$2.1 \cdot 10^{-2}$	$1.6 \cdot 10^{-12}$	$3.5 \cdot 10^{-10}$	$6.5 \cdot 10^{-10}$	34.0
IFC, tol $= 10^{-9}$	$2.1 \cdot 10^{-2}$	10^{-15}	$1.2 \cdot 10^{-9}$	$7.8 \cdot 10^{-10}$	14.5
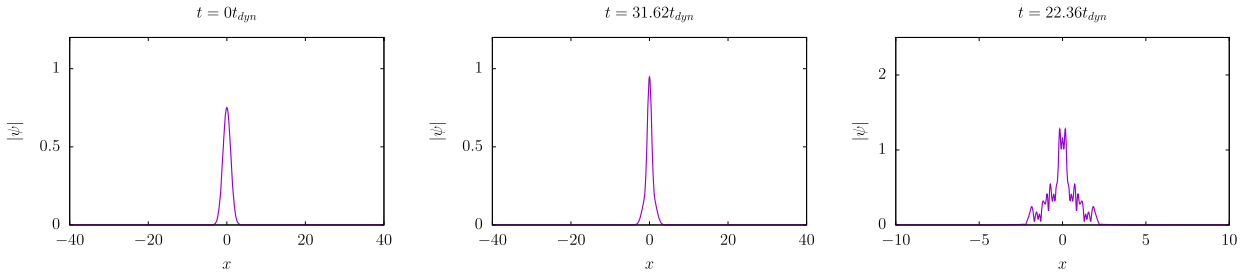
Fig. 1. Snapshots of the modulus of the solution of the 1D SN equation $|\psi|$. The left plot is the initial condition, center plot and right plot correspond to the solution at the end of the simulation for $g = 10$ and $g = 500$ respectively.

Table 2

Comparison for the 1D SN equation between the IFC method and the Split-Step solvers. The SSa simulations and IFC have been performed with a tolerance tol $= 10^{-7}$ and tol $= 10^{-10}$ respectively for $g = 10$ and tol $= 10^{-6}$ and tol $= 10^{-10}$ respectively for $g = 500$. The Δt for adaptive algorithms is the averaged one. T is the total time required to run each simulation, measured in seconds.

g	Method	$\Delta t / t_{\text{dyn}}$	$\overline{\Delta E}$	$\Delta \psi_{\text{rev}}$	$\Delta \psi_{\text{ref}}$	$T(s)$
10	SS2	$3.1 \cdot 10^{-4}$	$5.5 \cdot 10^{-10}$	$4.5 \cdot 10^{-11}$	$4.5 \cdot 10^{-9}$	123.3
	SS4	$6.3 \cdot 10^{-3}$	$2.9 \cdot 10^{-12}$	$2.5 \cdot 10^{-12}$	$5.5 \cdot 10^{-11}$	11.1
	SS6	$6.3 \cdot 10^{-2}$	$1.5 \cdot 10^{-13}$	$4.0 \cdot 10^{-12}$	$1.1 \cdot 10^{-11}$	3.5
	SSa	$4.3 \cdot 10^{-2}$	$4.2 \cdot 10^{-12}$	$8.5 \cdot 10^{-11}$	$5.9 \cdot 10^{-11}$	6.4
	IFC	$2.2 \cdot 10^{-2}$	$1.8 \cdot 10^{-12}$	$1.3 \cdot 10^{-10}$	$3.3 \cdot 10^{-11}$	5.0
500	SS2	10^{-5}	$6.0 \cdot 10^{-9}$	$1.1 \cdot 10^{-10}$	$5.2 \cdot 10^{-8}$	120.0
	SS4	$5 \cdot 10^{-4}$	$2.5 \cdot 10^{-9}$	$4.9 \cdot 10^{-12}$	$1.3 \cdot 10^{-7}$	5.4
	SS6	$2 \cdot 10^{-3}$	$1.8 \cdot 10^{-10}$	$2.8 \cdot 10^{-11}$	$7.6 \cdot 10^{-8}$	3.5
	SSa	$3.2 \cdot 10^{-2}$	$1.0 \cdot 10^{-10}$	$6.4 \cdot 10^{-8}$	$2.9 \cdot 10^{-8}$	6.7
	IFC	$5.4 \cdot 10^{-3}$	$1.8 \cdot 10^{-9}$	$2.3 \cdot 10^{-8}$	$1.5 \cdot 10^{-8}$	11.9

3.3. 1D Schrödinger–Newton equation

We now focus on the SN system, starting from the case of a single spatial dimension,

$$\mathrm{i}\frac{\partial \psi}{\partial t} + \frac{1}{2}\frac{\partial^2 \psi}{\partial x^2} - V\psi = 0, \qquad \frac{\partial^2 V}{\partial x^2} = g\,|\psi|^2. \tag{23}$$

The solutions of (23) depend on the initial condition and on the single parameter g. The chosen initial condition is $\psi(x, t = 0) = \exp(-x^2/2)/\sqrt[4]{\pi}$. The potential V is calculated using Hockney's method [37]. We perform a set of tests with different values of the parameter g, corresponding to different physical regimes. The case $g = 10$ corresponds to a system in the quantum regime, i.e., with an associated De Broglie wavelength of the order of the size of the system, while $g = 500$ corresponds to a system closer to the semi-classical regime, with an associated De Broglie wavelength about 20 times smaller than the size of the system. The typical evolution of this system is characterized by the initial condition which oscillates, exhibiting a complex dynamics. This is particularly visible in the semi-classical regime, in which high frequency oscillations appear in the wavefunction, as shown in Fig. 1. The simulation is run in a domain of length $L = 80$, discretized into $N = 2048$ points in the $g = 10$ case, while for $g = 500$ we set $L = 20$ and $N = 2048$ (Fig. 2). The characteristic time of dynamics is defined as $t_{\text{dyn}} = |g|^{-1/2}$. In Table 2, we compare the Split-Step integrators with the IFC, looking at the energy conservation error, the error on the solution and the total time needed to run each simulation. Here, splitting methods proved to be faster than the integrating factor. In addition, the SS4 and SS6 performed better than the adaptive integrators. This is due the fact that, for this particular system, the extra computational cost due to the implementation of the adaptive-step is not fully compensated by the time-gain in terms of computational speed. Indeed, splitting algorithms with fixed
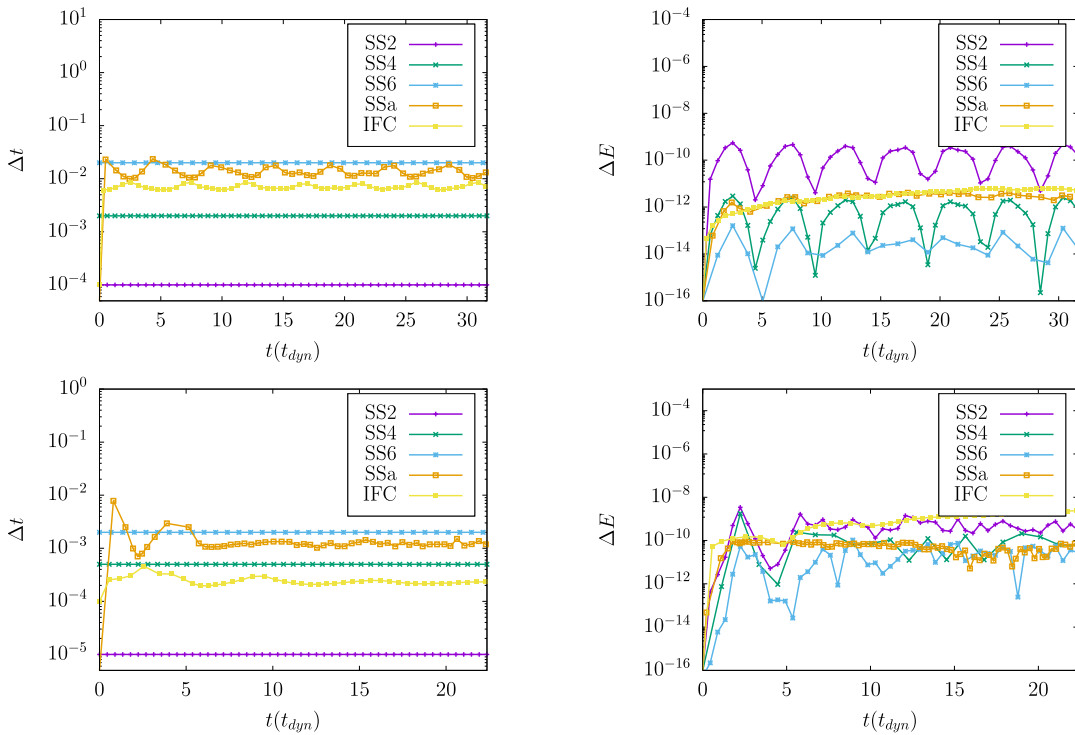
Fig. 2. Comparison for the 1D SN equation between the time-step and the error on the energy conservation for the IFC method and the Split-Step solvers for both the cases $g = 10$ (upper plots) and $g = 500$ (lower plots). (For interpretation of the colors in the figure(s), the reader is referred to the web version of this article.)

time-step require a smaller number of computational operations to be implemented. For this reason, here, choosing a "proper" fixed time-step still results in a slightly faster numerical integration compared to an adaptive scheme.

3.3.1. Periodical case

We now switch to another version of the SN system, which has important applications in cosmology in order to simulate the formation of large-scale structures in the universe (4). We take $a = 1$, which in cosmology corresponds to the case of a static universe [38]; we do not expect modifications of our conclusions for different cosmological models. In one dimension the equations read

$$i \frac{\partial \psi}{\partial t} + \frac{1}{2} \frac{\partial^2 \psi}{\partial x^2} - V \psi = 0, \tag{24a}$$

$$\frac{\partial^2 V}{\partial x^2} = g (|\psi|^2 - 1), \tag{24b}$$

where the wavefunction $|\psi|^2$ is normalized to unity. The potential V is obtained calculating the inverse of the Laplacian in Fourier space and transforming back the result to real space. We take "cold" initial conditions (see [39,40]), namely,

$$\psi(x, t = 0) = \sqrt{\rho_0 + \delta\rho(x)} \exp(i\theta(x)), \tag{25}$$

where θ is a function whose gradient is proportional to the initial velocity field (set to zero for simplicity), ρ_0 is the background constant density and $\delta\rho(x)$ is the density fluctuations, generated as

$$\delta\rho(x) = \mathcal{F}^{-1} \left[R(k) \sqrt{P(k)} \right], \tag{26}$$

where $R(k)$ is a Gaussian random field, with zero average and unity variance. The function $P(k)$ is called *Power Spectrum*, and it is defined as

$$P(k) = \frac{1}{L^d} \left| \widehat{\delta\rho}(k) \right|^2, \tag{27}$$

corresponding to the initial density fluctuations one wants to generate. The initial conditions are numerically initialized applying an additional filter $F(k)$ in Fourier space with the aim of setting to zero all the modes corresponding to a space scale comparable (or smaller) than the grid-step

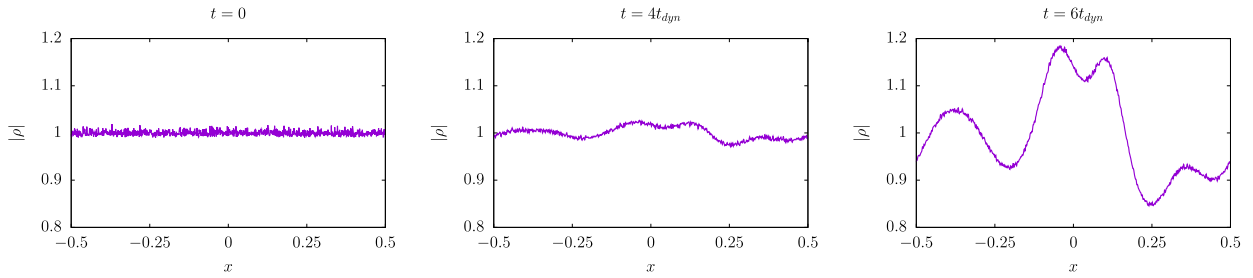$$F(k) = \text{sech} \left(\left(k/k_F \right)^{10} \right), \tag{28}$$

Fig. 3. Snapshots of the modulus squared of the solution of the 1D SN equation (periodical case) $|\psi|^2$.
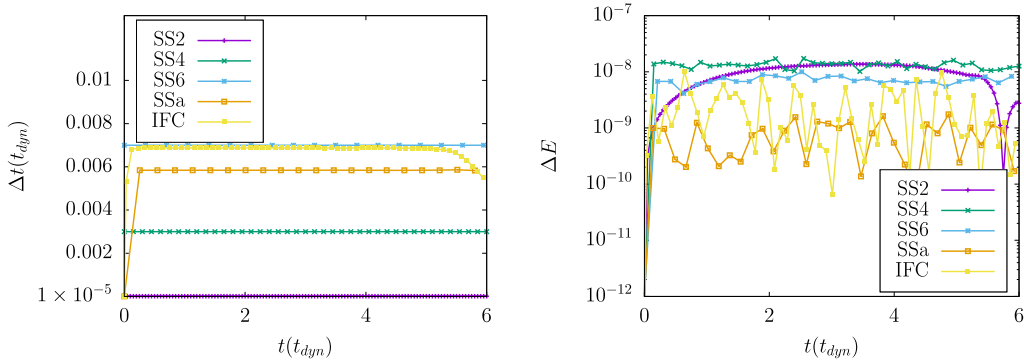

Fig. 4. Comparison for the 1D SN equation (periodical case) between the time-step (left plot) and the error on the energy conservation (right plot) for the IFC method and the Split-Step solvers.

Table 3
Comparison for the 1D SN equation (periodical case) between the IFC method and the Split-Step solvers. T is the total time required to run each simulation, measured in seconds. The Δt for adaptive algorithms is the averaged one.

Method	$\Delta t/t_{\mathrm{dyn}}$	$\overline{\Delta E}$	$\Delta\psi_{\mathrm{rev}}$	$\Delta\psi_{\mathrm{ref}}$	$T(s)$
SS2	10^{-5}	$1.6 \cdot 10^{-8}$	$8.3 \cdot 10^{-9}$	$8.5 \cdot 10^{-10}$	276.5
SS4	$3 \cdot 10^{-3}$	$1.9 \cdot 10^{-8}$	$1.3 \cdot 10^{-9}$	$1.5 \cdot 10^{-11}$	1.8
SS6	$7 \cdot 10^{-3}$	$1.1 \cdot 10^{-8}$	$1.1 \cdot 10^{-8}$	$3.1 \cdot 10^{-11}$	2.3
SSa, tol $= 10^{-9}$	$5.8 \cdot 10^{-3}$	$2.3 \cdot 10^{-9}$	$3.3 \cdot 10^{-9}$	$1.2 \cdot 10^{-11}$	4.3
IFC, tol $= 10^{-12}$	$6.7 \cdot 10^{-3}$	$1.1 \cdot 10^{-8}$	$1.8 \cdot 10^{-10}$	$6.7 \cdot 10^{-11}$	1.3

with $k_F = k_N/8$, where k_N is the Nyquist wavelength, defined as $k_N = \frac{N}{2L}$. Thus, the initial condition is

$$\psi(x,t=0) = \mathcal{F}^{-1}\left[F(k)\,\mathcal{F}\left[\sqrt{\rho_0 + \delta\rho(x)} \right] \right]. \tag{29}$$

In the simulations, space is discretized with $N = 1024$ points, in a domain of length $L = 1$ and a constant power spectrum is used as initial condition. We show the simulation results in the semi-classical regime. The latter corresponds to large values of the parameter g, as one has $g \propto \hbar^{-2}$. Specifically, we take $g = 10^6$ (we do not observe differences in the performance in the quantum regime, i.e., for smaller values of g) and $\rho_0 = 1$.

In Fig. 3, the typical evolution of the system in the cosmological context is shown: the initial condition is spatially homogeneous with small fluctuations. The fluctuations grow due to gravitational interactions, up to be dominated by the finite size of the simulation box. The characteristic time of dynamics is defined as $t_{\mathrm{dyn}} = |g|^{-1/2}$. In Fig. 4, the Split-Step integrators are compared with the IFC. We observe for $t \gtrsim 5t_{\mathrm{dyn}}$ that the time-step decreases; this is due to the fact that the dynamics switches from a regime where the largest scales are still linear, to a regime where all the scales are nonlinear [15]. It indicates that the integrating factor is particularly efficient in the weakly nonlinear regime, which is the regime of interest in cosmological simulations. The Split-Step integrators (except SS2) are observed to perform in the same manner in the weakly non-linear and strongly non-linear regime. We observe that IFC outperforms the tested Split-Step integrators in the first regime, whereas, in the second one it becomes equally efficient compared to the split-step methods. This is consistent with the observation of Sect. 3.3: since the dynamics corresponds to a highly nonlinear regime, the Split-Step method performs better than the IFC one in this case. Looking to Table 3, it is clear that (for the whole simulation of this system) the IFC is the most efficient integration method.
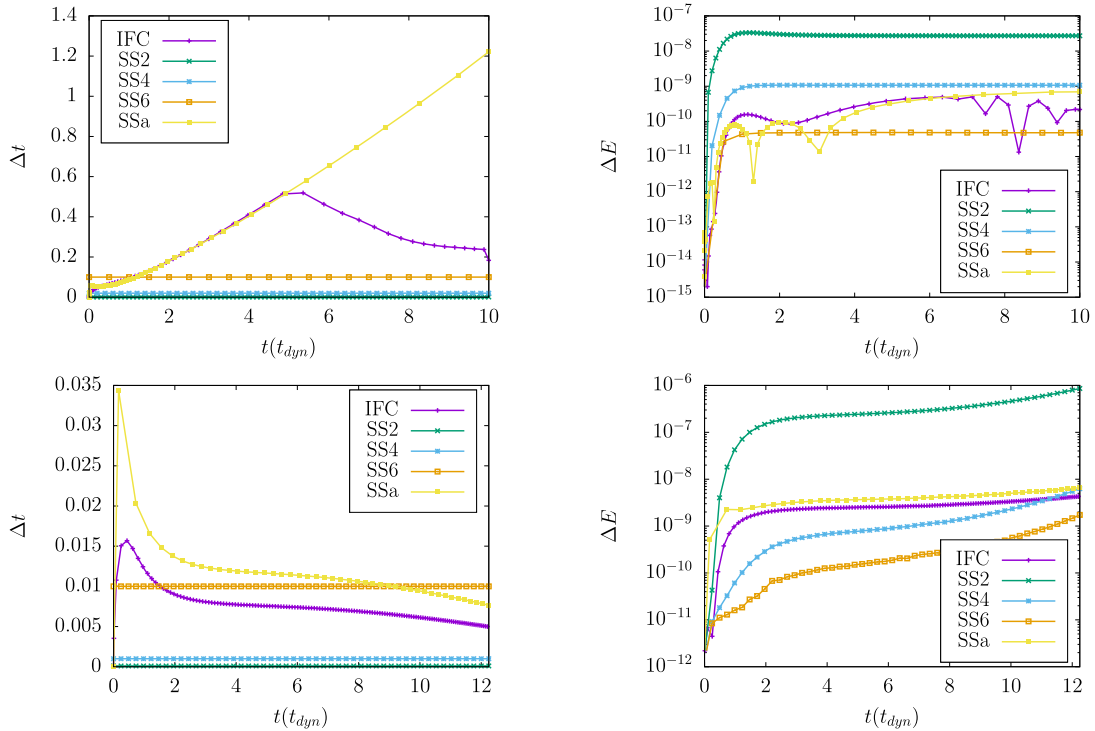
Fig. 5. Comparison for the 2D NLS equation between the time-step (left panel) and the error on the energy conservation (right panel) for the IFC method and the Split-Step solvers. The top row corresponds to the $g = -1$ case while the bottom row to $g = -6$. The last time-step is chosen in such a way that the final time is the same in all simulations, in order to ensure that $\Delta\psi_{\text{rev}}$ and $\Delta\psi_{\text{ref}}$ are evaluated properly, which explain the step which appears for the last time point in Δt.

3.4. 2D nonlinear Schrödinger equation

In the 2D NLS case, one has

$$i\,\partial_t\,\psi \;+\; \tfrac{1}{2}\,\nabla^2\,\psi \;-\; g\,|\psi|^2\,\psi \;=\; 0. \tag{30}$$

The dynamics of (30) presents a finite time singularity: it can be proven [41] that there exists a finite time when the norm of the solution or of one of its derivatives becomes infinity. This happens whenever the initial condition ψ_0 satisfies $E_g = \frac{1}{2}\int d\mathbf{r}\,\psi_0\left(g\,|\psi_0|^2 - \nabla^2\right)\psi_0^* < 0$. The initial condition is taken as $\psi(\mathbf{r}, t = 0) = e^{-r^2/2}/\sqrt{\pi}$ and we study the cases $g = -1$ and $g = -6$ with respective initial energies $E_{g=-1} \approx 0.42$ and $E_{g=-6} \approx 0.02$. Thus, the latter is associated with an initial energy closer to the singular regime than the former. The simulation is run in a box of side $L = 80$, discretized into $N = 1024 \times 1024$ points in the $g = -1$ case, while for $g = -6$ we set $L = 120$ and $N = 4096 \times 4096$. The characteristic time of dynamics is defined as $t_{\text{dyn}} = |g|^{-1/2}$.

Split-Step integrators are compared with the IFC, looking at the energy conservation error, the error on the solution and the total time needed to run each simulation. The results are illustrated in Fig. 5 and Table 4. The gain factor between splitting algorithms and the IFC method depends on the value of g. However, in both cases, the optimized integrating factor proved to be more efficient.

3.5. 2D Schrödinger-Newton equation

In the 2D SN case, one has

$$i\,\partial_t\,\psi \;+\; \tfrac{1}{2}\,\nabla^2\,\psi \;-\; V\,\psi \;=\; 0, \qquad \nabla^2 V \;=\; g\,|\psi|^2. \tag{31}$$

Similarly to the one dimensional case, we use a Gaussian initial conditions $\psi(\mathbf{r}, t = 0) = e^{-r^2/2}/\sqrt{\pi}$ and two values of the coupling constant, $g = 10$ and $g = 500$. The former corresponds to a system in the quantum regime and the latter is closer to the semi-classical one. The potential V, as in the 1D case, is calculated using the Hockney method [37]. The simulation is run in a box of side $L = 40$, discretized into $N = 1024^2$ points in the $g = 10$ case, while for $g = 500$ we set $L = 20$ and $N = 1024 \times 1024$, the characteristic time of dynamics is defined as $t_{\text{dyn}} = |g|^{-1/2}$.

In Table 5 and Fig. 6, we compare the Split-Step and the IFC integrators, looking at the energy conservation error, the error on the solution and the total time needed to run each simulation.

For the 2D Schrödinger–Newton equation, adaptive splitting algorithms proved to be as efficient as the IFC. Similarly to the one-dimensional case, also here the SS6 split-step algorithm with constant time-step resulted to be the fastest among the ones we

Table 4
Comparisons for the 2D NLS equation between different methods for the Dormand and Prince integrator. The Δt for adaptive algorithms is the averaged one. T is the total time required to run each simulation, measured in seconds. The tolerances of the integrator SS4(3) is tol $= 10^{-6}$ and tol $= 10^{-10}$ for the IFC.

g	Method	$\Delta t/t_{\mathrm{dyn}}$	$\overline{\Delta E}$	$\Delta\psi_{\mathrm{rev}}$	$\Delta\psi_{\mathrm{ref}}$	$T(s)$
-1	SS2	10^{-3}	$3.3\cdot10^{-8}$	$4.5\cdot10^{-8}$	$5.0\cdot10^{-10}$	6939
	SS4	$2\cdot10^{-2}$	$1.1\cdot10^{-9}$	$3.5\cdot10^{-13}$	$7.0\cdot10^{-11}$	830
	SS6	10^{-1}	$4.5\cdot10^{-11}$	$2.5\cdot10^{-14}$	$6.2\cdot10^{-11}$	445
	SSa	$2.3\cdot10^{-1}$	$7.0\cdot10^{-10}$	$3.0\cdot10^{-10}$	$2.5\cdot10^{-11}$	267
	IFC	$1.7\cdot10^{-1}$	$4.5\cdot10^{-10}$	$3.0\cdot10^{-10}$	$1.6\cdot10^{-11}$	169
-6	SS2	$2.5\cdot10^{-4}$	$8.8\cdot10^{-7}$	$1.4\cdot10^{-11}$	$7.9\cdot10^{-7}$	405012
	SS4	$2.5\cdot10^{-3}$	$6.3\cdot10^{-9}$	$2.5\cdot10^{-12}$	$3.7\cdot10^{-9}$	82891
	SS6	$2.5\cdot10^{-2}$	$1.7\cdot10^{-9}$	$1.6\cdot10^{-12}$	$1.8\cdot10^{-9}$	24453
	SSa	$2.8\cdot10^{-2}$	$6.5\cdot10^{-9}$	$1.4\cdot10^{-10}$	$5.4\cdot10^{-9}$	29117
	IFC	$1.8\cdot10^{-2}$	$2.3\cdot10^{-9}$	$3.5\cdot10^{-9}$	$9.4\cdot10^{-9}$	22843

Table 5
Comparison for the 2D SN equation between the IFC method and the Split-Step solvers. The Δt for adaptive algorithms is the averaged one. The tolerance for the SSa algorithm is tol $= 10^{-6}$ and tol $= 10^{-7}$ for $g = 10$ and $g = 500$ respectively, and for the IFC algorithm tol $= 10^{-10}$ and tol $= 10^{-12}$ for $g = 10$ and $g = 500$ respectively.

g	Method	$\Delta t/t_{\mathrm{dyn}}$	$\overline{\Delta E}$	$\Delta\psi_{\mathrm{rev}}$	$\Delta\psi_{\mathrm{ref}}$	$T(s)$
10	SS2	$3.2\cdot10^{-3}$	$1.8\cdot10^{-8}$	$3.5\cdot10^{-12}$	$1.0\cdot10^{-7}$	9070
	SS4	$6.3\cdot10^{-2}$	$6.0\cdot10^{-10}$	$1.4\cdot10^{-11}$	$3.8\cdot10^{-8}$	959
	SS6	$1.9\cdot10^{-1}$	$4.6\cdot10^{-11}$	$1.6\cdot10^{-7}$	$4.1\cdot10^{-8}$	932
	SSa	$1.7\cdot10^{-1}$	$4.7\cdot10^{-11}$	$1.4\cdot10^{-7}$	$3.9\cdot10^{-8}$	1174
	IFC	$8.4\cdot10^{-2}$	$1.3\cdot10^{-10}$	$5.8\cdot10^{-8}$	$2.9\cdot10^{-8}$	1172
500	SS2	$2.2\cdot10^{-4}$	$2.0\cdot10^{-8}$	$3.1\cdot10^{-10}$	$9.1\cdot10^{-8}$	84030
	SS4	$4.5\cdot10^{-3}$	$5.6\cdot10^{-10}$	$2.8\cdot10^{-11}$	$7.0\cdot10^{-9}$	8401
	SS6	$2.2\cdot10^{-2}$	$6.1\cdot10^{-12}$	$9.1\cdot10^{-11}$	$4.1\cdot10^{-9}$	5143
	SSa	$2.1\cdot10^{-2}$	$1.9\cdot10^{-11}$	$2.0\cdot10^{-11}$	$3.9\cdot10^{-9}$	6676
	IFC	$9.1\cdot10^{-3}$	$7.5\cdot10^{-11}$	$3.0\cdot10^{-10}$	$1.6\cdot10^{-9}$	6637

tested. This is due to the same reasons mentioned in section 3.3. Note that, here, the performance gap between the integrating factor and splitting algorithms is smaller than in the one-dimensional case. Indeed, as the dynamics gets more complicated and the number of spatial dimensions increase, algorithms with adaptive time-step shall always be preferred.

3.5.1. Periodical case

For the 2D periodical case, we run simulations in a box of side $L = 1$ with $N = 1024 \times 1024$, using again a constant power spectrum as initial condition with $g = 10^6$, $\rho_0 = 1$ and a zero initial velocity field. In Fig. 7 some snapshots of the modulus squared of the solution are shown, expressing time in units of $t_{\mathrm{dyn}} = 1/\sqrt{g}$.

In Table 6 and Fig. 8, we compare the Split-Step and IFC integrators, looking at the energy conservation error, the error on the solution and the total time needed to run each simulation. We obtain the same result than in one dimension, with the IFC being the most efficient method.

3.6. Gross–Pitaevskii–Poisson equation

We conclude by presenting the results for the 2D Gross–Pitaevskii–Poisson equation, which is a combination of the NLS and SN equations

$$\mathrm{i}\,\partial_t\,\psi \;+\; \frac{1}{2}\nabla^2\,\psi \;-\; V\,\psi \;=\; 0, \qquad V = V_1 + V_2, \qquad \nabla^2 V_1 = g_1\,|\psi|^2, \qquad V_2 = g_2\,|\psi|^2.$$

Based on the results presented so far, in the case of open boundary conditions, one expects the split-step or the integrating factors to outperform one the other, depending on the values of g_1 and g_2. We set them to $g_1 = -3$ and $g_2 = 100$ which are very close to the one typically employed when simulating the collapse of a self-gravitating Bose-Einstein condensate with attractive self-interaction [21]. The numerical parameters are $N = 2048 \times 2048$, $L = 40$ and $t_f = 5$ while the initial condition is a Gaussian, $\psi(\boldsymbol{r}, t = 0) = \mathrm{e}^{-r^2/2}/\sqrt{\pi}$. In Table 7 comparisons between the most efficient methods tested for the NLS (IFC method) and the SN in the non-periodical case (SS6 or SSa, depending on the parameters) are shown. We checked that the SS6 method continues to demonstrate superior performance compared to SS2 and SS4, as shown in all the other 2D cases. We observe that for our particular initial condition, and values of g_1 and g_2, the IFC method outperforms the split-step solvers.
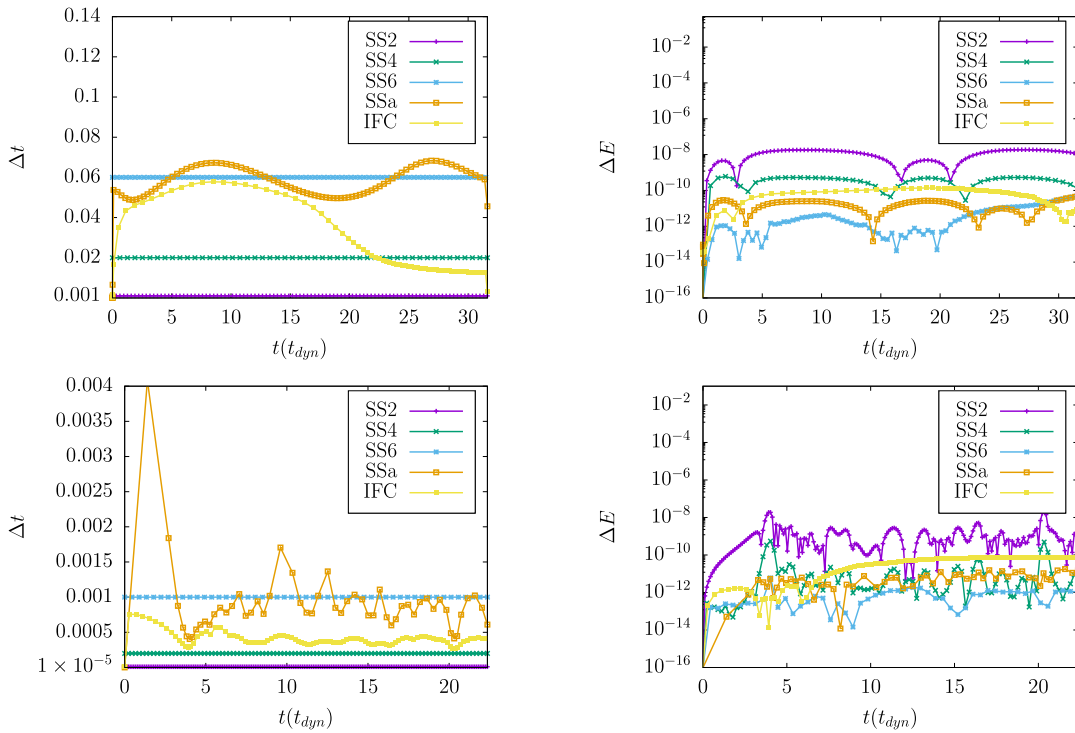
Fig. 6. Comparison for the 2D SN equation between the time-step and the error on the energy conservation with the IFC method and the Split-Step solvers for both the cases $g = 10$ (upper plots) and $g = 500$ (lower plots).
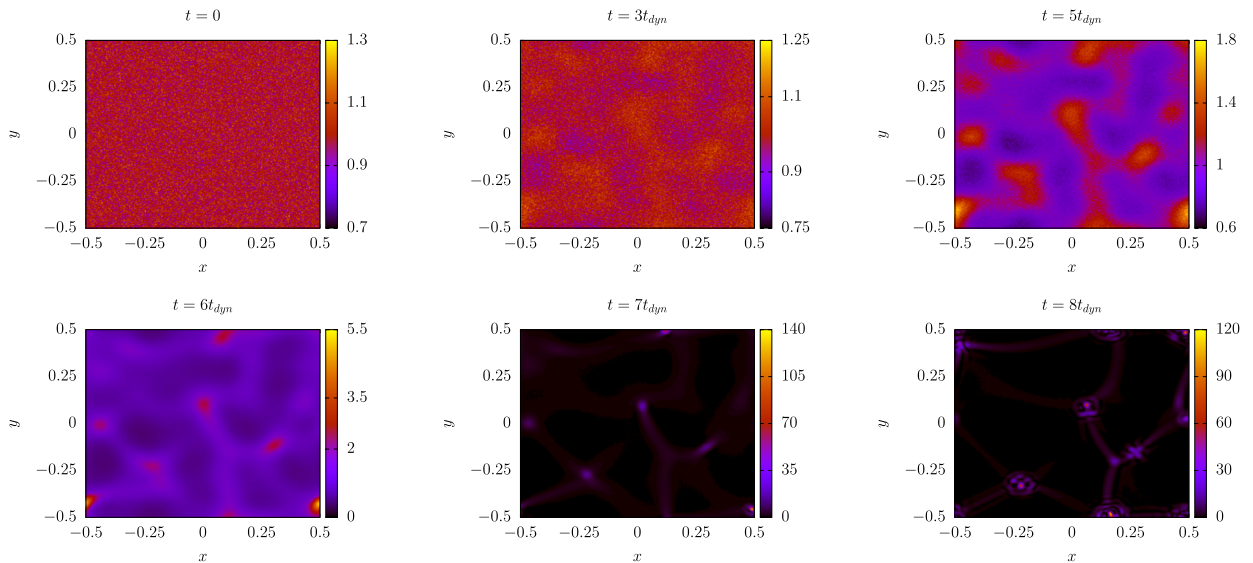

**Fig. 7.** Snapshots of the modulus squared of the solution of the 2D SN equation (periodical case) $|\psi|^2$.

4. Conclusion

We studied the numerical resolution of the nonlinear Schrödinger (NLS) and the Newton–Schrödinger (SN) equations using the optimized integrating factor (IFC) technique. This method was compared with splitting algorithms. Specifically, for the integrating factor, we tested fifth-order time-adaptive algorithms, while, for the Split-Step family, we focused on second-, fourth- and sixth-order schemes with fixed time-step, and a fourth-order algorithm with adaptive time-step. We performed extensive tests with systems in one and two spatial dimensions, with open or periodic boundary conditions.

Table 6

Comparison for the 2D SN equation (periodical case) between the IFC method and the Split-Step solvers. T is the total time required to run each simulation, measured in seconds. The Δt for adaptive algorithms is the averaged one.

Method	$\Delta t/t_{\mathrm{dyn}}$	$\overline{\Delta E}$	$\Delta\psi_{rev}$	$\Delta\psi_{ref}$	$T(s)$
SS2	10^{-4}	$1.8\cdot 10^{-8}$	$4.5\cdot 10^{-9}$	$1.0\cdot 10^{-5}$	31711
SS4	$3\cdot 10^{-3}$	$4.2\cdot 10^{-8}$	$3.1\cdot 10^{-6}$	$5.3\cdot 10^{-6}$	2485
SS6	$7\cdot 10^{-3}$	$3.5\cdot 10^{-8}$	$4.5\cdot 10^{-10}$	$5.1\cdot 10^{-6}$	3046
SSa, tol $=10^{-7}$	$7.5\cdot 10^{-3}$	$2.3\cdot 10^{-7}$	$8.5\cdot 10^{-7}$	$1.2\cdot 10^{-6}$	3362
IFC, tol $=10^{-12}$	$5\cdot 10^{-3}$	$9.5\cdot 10^{-8}$	$4.6\cdot 10^{-6}$	$8.9\cdot 10^{-7}$	2232
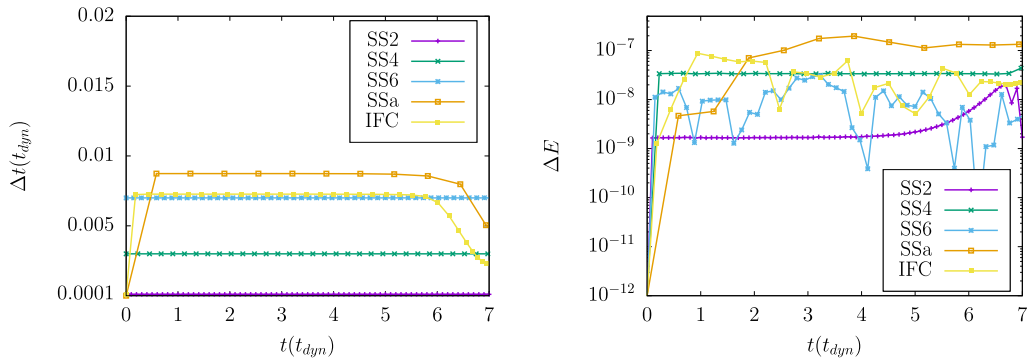
Fig. 8. Comparison for the 2D SN equation (periodical case) between the time-step (left plot) and the error on the energy conservation (right plot) for the IFC method and the Split-Step solvers.

Table 7

Comparison for the 2D Gross–Pitaevskii–Poisson equation between the IFC and the Split-Step methods. T is the total time required to run each simulation, measured in seconds.

Method	Δt	$\overline{\Delta E}$	$\Delta\psi_{rev}$	$\Delta\psi_{ref}$	$T(s)$
SS6	$2.5\cdot 10^{-3}$	$1.2\cdot 10^{-9}$	$4.5\cdot 10^{-11}$	$4.5\cdot 10^{-8}$	32753
SSa, tol $=10^{-7}$	$4\cdot 10^{-3}$	$2.4\cdot 10^{-11}$	$2.2\cdot 10^{-8}$	$1.4\cdot 10^{-8}$	63315
IFC, tol $=10^{-11}$	$2\cdot 10^{-3}$	$7.7\cdot 10^{-10}$	$6.2\cdot 10^{-8}$	$2.3\cdot 10^{-8}$	28273

The comparisons between the results obtained in the tested cases, show that the IFC method can be more efficient than splitting algorithms, especially in the NLS equation and periodical SN equation cases. For the SN equation in the non-periodical case on the other hand, splitting algorithms proved to be more efficient, even though the optimized integrating factor provided competitive results in terms of both speed and accuracy. Moreover, the results obtained for the Gross–Pitaevskii–Poisson equation pointed out how, for the particular values of the parameters we tested, the presence of a short-range interaction term puts the integrating factor method in a clear more performing position.

Finally, the achieved results indicate how, among the splitting algorithms at fixed step, working with higher order solvers is always more efficient. In particular the Split-Step order 6 proved to be around 10 times faster compared with the lower order ones, while conserving the energy with the same error.

Appendix A. Optimized integrating factor

The optimized version of the integrating factor is based on the property that, for the Schrödinger equation, if the value of the potential V is modified by an additive constant C, only the phase of the solution ψ is changed. Indeed, if ψ is a solution of (1) at a given time t, then $\Psi \overset{\mathrm{def}}{=} \psi\,\mathrm{e}^{-\mathrm{i}Ct}$ is a solution of

$$\mathrm{i}\,\partial_t\,\Psi \;+\; \tfrac{1}{2}\,\nabla^2\Psi \;-\; (V+C)\,\Psi \;=\; 0, \tag{A.1}$$

as it can be easily verified. Thus, adding a constant C_n to V, the solution is modified as

$$\psi(t_n)\;\to\;\psi(t_n)\,\mathrm{e}^{-\mathrm{i}\varphi}, \qquad \varphi \overset{\mathrm{def}}{=} \sum_{n=0}^{N_h} C_n\,h_n, \tag{A.2}$$

where $h_n \overset{\mathrm{def}}{=} t_{n+1} - t_n$ is the n-th time-step and N_h is the total number of time-steps.

The freedom provided by the gauge condition of the potential is exploited to compute an optimal value of C_n, which allows to choose a larger time-step compared to the $C_n = 0$ case and therefore speeding up the numerical integration. The resulting optimal value, $\tilde{C}_n$, which is obtained at each time step n as the value of C_n minimizing the L_2-norm of $\mathcal{N}$ [32], is

$$
\tilde{C}_n \stackrel{\text{def}}{=} -\left(\sum_{\ell=-[M/2]}^{[M/2]-1} V_\ell \, |\psi_\ell|^2 \right) \Bigg/ \left(\sum_{\ell=-[M/2]}^{[M/2]-1} |\psi_\ell|^2 \right)
\tag{A.3}
$$

where $\psi_\ell \stackrel{\text{def}}{=} \psi(\boldsymbol{r}_\ell)$ and $V_\ell \stackrel{\text{def}}{=} V(\boldsymbol{r}_\ell)$ at time t_n.

Appendix B. Split-Step pseudo-codes

We list below, in Algorithm 1, the pseudo-codes for the Split-Step algorithms with fixed time-step. We consider the general case of order N, with $N \in \{2, 4, 6\}$.

Algorithm 1 SSN, $N \in \{2, 4, 6\}$.

1: $t \leftarrow t_0$
2: $\psi \leftarrow \psi(\boldsymbol{r}, t_0)$
3: **while** $t < t_f$ **do**
4:     $\psi \leftarrow \text{FFT}^{-1}[\exp(-i\hat{K}a_1 h)\,\text{FFT}[\psi]]$
5:     $\psi \leftarrow \exp(-iVb_1 h)\,\psi$
6:     $\vdots$
7:     $\psi \leftarrow \text{FFT}^{-1}[\exp(-i\hat{K}a_{\frac{N}{2}} h)\,\text{FFT}[\psi]]$
8:     $\psi \leftarrow \exp(-iVb_{\frac{N}{2}} h)\,\psi$
9:     $\psi \leftarrow \text{FFT}^{-1}[\exp(-i\hat{K}a_{\frac{N}{2}-1} h)\,\text{FFT}[\psi]]$
10:    $\psi \leftarrow \exp(-iVb_{\frac{N}{2}-1} h)\,\psi$
11:    $\vdots$
12:    $\psi \leftarrow \text{FFT}^{-1}[\exp(-i\hat{K}a_1 h)\,\text{FFT}[\psi]]$
13:    $\psi \leftarrow \exp(-iVb_1 h)\,\psi$
14:    $t \leftarrow t + h$

In the latter, h is the time step, FFT and FFT^{-1} denote the Fast Fourier Transform and its inverse respectively, $\hat{K}$ is the kinetic energy operator in Fourier space, V is the potential, and the values of a_i and b_i, $i \in \{1, 2, 3, 4, 5, 6\}$, are listed in Table B.8.

Table B.8
Values of the parameters for the Split-Step algorithms. The quantity ω is given by $\omega = \frac{2 + 2^{\frac{1}{3}} + 2^{-\frac{1}{3}}}{3}$.

SS2	SS4	SS6
$a_1 = \frac{1}{2}$	$a_1 = \frac{\omega}{2}$	$a_1 = 0.0502627644003922$
$b_1 = 1$	$b_1 = 1$	$b_1 = 0.148816447901042$
	$a_2 = \frac{1-\omega}{2}$	$a_2 = 0.413514300428344$
	$b_2 = 1 - 2\omega$	$b_2 = -0.132385865767784$
		$a_3 = 0.0450798897943977$
		$b_3 = 0.067307604692185$
		$a_4 = -0.188054853819569$
		$b_4 = 0.432666402578175$
		$a_5 = 0.541960678450780$
		$b_5 = 0.5 - (b_1 + b_2 + b_3 + b_4)$
		$a_6 = 1 - 2(a_1 + a_2 + a_3 + a_4 + a_5)$
		$b_6 = 1 - 2(a_1 + a_2 + a_3 + a_4 + a_5)$

In the case of SSa, the adaptive splitting algorithm, i.e. the SS4(3), both the solutions at the 4th and at the 3rd order must be evaluated. The pseudo-code is described in Algorithm 2, while the coefficients are listed in B.9. In our numerical tests we set $\alpha = 0.9$, $\beta = 3$.

Algorithm 2 SSa.

1: $t \leftarrow t_0$
2: $\psi \leftarrow \psi(\boldsymbol{r}, t_0)$
3: **while** $t < t_f$ **do**
4:     $\psi \leftarrow \widetilde{\psi}$
5:     $\psi \leftarrow \text{FFT}^{-1}[e^{-i\hat{K}a_1 h}\text{FFT}[\psi]]$
6:     $\psi \leftarrow e^{-iVb_1 h}\psi$
7:     $\vdots$
8:     $\psi \leftarrow \text{FFT}^{-1}[e^{-i\hat{K}a_7 h}\text{FFT}[\psi]]$
9:     $\psi \leftarrow e^{-iVb_7 h}\psi$
10:    $\widetilde{\psi} \leftarrow \text{FFT}^{-1}[e^{-i\hat{K}\bar{a}_1 h}\text{FFT}[\widetilde{\psi}]]$
11:    $\widetilde{\psi} \leftarrow e^{-iV\bar{b}_1 h}\widetilde{\psi}$
12:    $\vdots$
13:    $\widetilde{\psi} \leftarrow \text{FFT}^{-1}[e^{-i\hat{K}\bar{a}_7 h}\text{FFT}[\widetilde{\psi}]]$
14:    $\widetilde{\psi} \leftarrow e^{-iV\bar{b}_7 h}\widetilde{\psi}$
15:    $err \leftarrow \sqrt{\dfrac{\sum_{i=1}^{N}|\psi(\boldsymbol{x}_i, t_n) - \widetilde{\psi}(\boldsymbol{x}_i, t_n)|^2}{\sum_{j=1}^{N}|\psi(\boldsymbol{x}_j, t_n)|^2}}$
16:    **if** $err \leq \text{tol}$ **then**
17:      $t \leftarrow t + h$
18:    **else**
19:      $\psi \leftarrow \widetilde{\psi}$
20:    $h \leftarrow h \min\left\{ \alpha\left(\dfrac{\text{tol}}{\Delta_n}\right)^{\frac{1}{4}}, \beta \right\}$

Table B.9
Values of the parameters for the SSa.

SSa			
Order 4		Order 3	
a_1	0	$\bar{a}_1$	0
b_1	0.0829844064174052	$\bar{b}_1$	0.0829844064174052
a_2	0.245298957184271	$\bar{a}_2$	0.245298957184271
b_2	0.3963098014983680	$\bar{b}_2$	0.3963098014983680
a_3	0.604872665711080	$\bar{a}_3$	0.604872665711080
b_3	-0.0390563049223486	$\bar{b}_3$	-0.0390563049223486
a_4	0.5 - $(a_2 + a_3)$	$\bar{a}_4$	0.5 - $(a_2 + a_3)$
b_4	1. - $2(b_1 + b_2 + b_3)$	$\bar{b}_4$	1. - $2(b_1 + b_2 + b_3)$
a_5	0.5 - $(a_2 + a_3)$	$\bar{a}_5$	0.3752162693236828
b_5	-0.03905630492223486	$\bar{b}_5$	0.4463374354420499
a_6	0.604872665711080	$\bar{a}_6$	1.4878666594737946
b_6	0.3963098014983680	$\bar{b}_6$	-0.0060995324486253
a_7	0.245298957184271	$\bar{a}_7$	-1.3630829287974774
b_7	0.0829844064174052	$\bar{b}_7$	0

References

[1] F. Dalfovo, S. Giorgini, L.P. Pitaevskii, S. Stringari, Theory of Bose–Einstein condensation in trapped gases, Rev. Mod. Phys. 71 (3) (1999) 463.
[2] A. Hasegawa, Optical solitons in fibers, in: Optical Solitons in Fibers, Springer, 1989, pp. 1–74.
[3] C. Kharif, E. Pelinovsky, A. Slunyaev, Rogue Waves in the Ocean, Springer Science & Business Media, 2008.
[4] J. Binney, S. Tremaine, Galactic Dynamics, second edition, 2008.
[5] F. Dabby, J. Whinnery, Thermal self-focusing of laser beams in lead glasses, Appl. Phys. Lett. 13 (8) (1968) 284–286.
[6] C. Rotschild, O. Cohen, O. Manela, M. Segev, T. Carmon, Solitons in nonlinear media with an infinite range of nonlocality: first observation of coherent elliptic solitons and of vortex-ring solitons, Phys. Rev. Lett. 95 (21) (2005) 213904.
[7] C. Rotschild, B. Alfassi, O. Cohen, M. Segev, Long-range interactions between optical solitons, Nat. Phys. 2 (11) (2006) 769–774.
[8] F.S. Guzman, L.A. Urena-Lopez, Gravitational cooling of self-gravitating Bose condensates, Astrophys. J. 645 (2) (2006) 814.
[9] W. Hu, R. Barkana, A. Gruzinov, Fuzzy cold dark matter: the wave properties of ultralight particles, Phys. Rev. Lett. 85 (6) (2000) 1158.
[10] A. Paredes, H. Michinel, Interference of dark matter solitons and galactic offsets, Phys. Dark Universe 12 (2016) 50–55.
[11] D.J. Marsh, J.C. Niemeyer, Strong constraints on fuzzy dark matter from ultrafaint dwarf galaxy Eridanus ii, Phys. Rev. Lett. 123 (5) (2019) 051103.
[12] L. Diosi, Gravitation and quantum-mechanical localization of macroobjects, preprint, arXiv:1412.0201.
[13] R. Penrose, On gravity's role in quantum state reduction, Gen. Relativ. Gravit. 28 (5) (1996) 581–600.
[14] L.M. Widrow, N. Kaiser, Using the Schrödinger equation to simulate collisionless matter, Astrophys. J. 416 (1993) L71.
[15] P.J.E. Peebles, The Large-Scale Structure of the Universe, 1980.
[16] N. Banik, A.J. Christopherson, P. Sikivie, E.M. Todarello, Linear Newtonian perturbation theory from the Schrödinger–Poisson equations, Phys. Rev. D 91 (12) (2015) 123540, https://doi.org/10.1103/PhysRevD.91.123540.
[17] C. Conti, M. Peccianti, G. Assanto, Route to nonlocality and observation of accessible solitons, Phys. Rev. Lett. 91 (7) (2003) 073901.
[18] Y. Izdebskaya, W. Krolikowski, N.F. Smyth, G. Assanto, Vortex stabilization by means of spatial solitons in nonlocal media, J. Opt. 18 (5) (2016) 054006.
[19] D. O'dell, S. Giovanazzi, G. Kurizki, V. Akulin, Bose–Einstein condensates with $1/r$ interatomic attraction: electromagnetically induced "gravity", Phys. Rev. Lett. 84 (25) (2000) 5687.

[20] A. Suárez, P.-H. Chavanis, Cosmological evolution of a complex scalar field with repulsive or attractive self-interaction, Phys. Rev. D 95 (6) (2017) 063515.

[21] P.-H. Chavanis, Collapse of a self-gravitating Bose–Einstein condensate with attractive self-interaction, Phys. Rev. D 94 (8) (2016) 083007.

[22] A. Bernal, F.S. Guzman, Scalar field dark matter: head-on interaction between two structures, Phys. Rev. D 74 (10) (2006) 103002.

[23] M. Thalhammer, High-order exponential operator splitting methods for time-dependent Schrödinger equations, SIAM J. Numer. Anal. 46 (4) (2008) 2022–2038.

[24] H. Holden, K.H. Karlsen, K.-A. Lie, Splitting Methods for Partial Differential Equations with Rough Solutions: Analysis and MATLAB Programs, vol. 11, European Mathematical Society, 2010.

[25] P. Bader, S. Blanes, F. Casas, M. Thalhammer, Efficient time integration methods for Gross–Pitaevskii equations with rotation term, preprint, arXiv:1910.12097.

[26] C. Besse, G. Dujardin, I. Lacroix-Violet, High order exponential integrators for nonlinear Schrödinger equations with application to rotating Bose–Einstein condensates, SIAM J. Numer. Anal. 55 (3) (2017) 1387–1411.

[27] J.R. Dormand, P.J. Prince, A family of embedded Runge–Kutta formulae, J. Comput. Appl. Math. 6 (1) (1980) 19–26.

[28] C. Tsitouras, Runge–Kutta pairs of order 5(4) satisfying only the first column simplifying assumption, Comput. Math. Appl. 62 (2) (2011) 770–775.

[29] R. Alexander, Solving ordinary differential equations i: Nonstiff problems (e. hairer, sp norsett, and g. wanner), SIAM Rev. 32 (3) (1990) 485.

[30] C. Canuto, M.Y. Hussaini, A. Quarteroni, T.A. Zang, Spectral Methods. Fundamentals in Single Domains, 2nd edition, Scientific Computation, Springer, 2008.

[31] J.C. Butcher, Numerical Methods for Ordinary Differential Equations, John Wiley & Sons, 2016.

[32] M. Lovisetto, D. Clamond, B. Marcos, Optimized integrating factor technique for Schrödinger-like equations, Appl. Numer. Math. 178 (2022) 329–336.

[33] S. Blanes, F. Casas, A. Murua, Splitting and composition methods in the numerical integration of differential equations, preprint, arXiv:0812.0377.

[34] M. Suzuki, General theory of fractal path integrals with applications to many-body theories and statistical physics, J. Math. Phys. 32 (2) (1991) 400–407.

[35] M. Thalhammer, J. Abhau, A numerical study of adaptive space and time discretisations for Gross–Pitaevskii equations, J. Comput. Phys. 231 (20) (2012) 6665–6681.

[36] S. Blanes, P.C. Moan, Practical symplectic partitioned Runge–Kutta and Runge–Kutta–Nyström methods, J. Comput. Appl. Math. 142 (2) (2002) 313–330.

[37] R.W. Hockney, J.W. Eastwood, Computer Simulation Using Particles, CRC Press, 2021.

[38] S. Weinberg, Cosmology, OUP, Oxford, 2008.

[39] G. Davies, L.M. Widrow, Test-bed simulations of collisionless, self-gravitating systems using the Schrödinger method, Astrophys. J. 485 (2) (1997) 484–495, https://doi.org/10.1086/304440.

[40] P. Mocz, L. Lancaster, A. Fialkov, F. Becerra, P.-H. Chavanis, Schrödinger–Poisson Vlasov–Poisson correspondence, Phys. Rev. D 97 (2018) 083519, https://doi.org/10.1103/PhysRevD.97.083519, https://link.aps.org/doi/10.1103/PhysRevD.97.083519.

[41] C. Sulem, P.-L. Sulem, The Nonlinear Schrödinger Equation: Self-Focusing and Wave Collapse, vol. 139, Springer Science & Business Media, 2007.